PULMONARY LOBE SEGMENTATION FROM CT IMAGES USING FISSURENESS, AIRWAYS, VESSELS AND MULTILEVEL B-SPLINES

Tom Doel[1], Tahreema N. Matin[2], Fergus V. Gleeson[2], David J. Gavaghan[1] and Vicente Grau[3]

[1]Department of Computer Science, University of Oxford, [2]Department of Radiology, Churchill Hospital, Oxford, [3]Department of Engineering Science and Oxford e-Research Centre, University of Oxford, UK.

ABSTRACT

Lobe detection from CT images is a challenging segmentation problem with important respiratory health care applications, including surgical planning and regional image analysis. We present a fully automated method for segmenting the pulmonary lobes. We first build a lobar approximation by applying a watershed transform to a vesselness density filter, using seed points generated from segmentation and analysis of the bronchial tree. We then apply a fissureness filter, which combines Hessian-based detection of planar structures with suppression of locally fissure-like points on the boundaries of the pulmonary vasculature. Finally, we fit a smooth multi-level B-spline curve through the fissureness maxima and extrapolate to the lung boundaries. Our method addresses several limitations of similar work, namely it is robust to incomplete fissures and vessels crossing the lobar boundaries, and it is computationally efficient and does not require training. We provide validation using fissure landmarks manually placed on 10 lung cancer datasets by a pulmonary clinician.

Index Terms— Computed tomography (CT), fissures, lungs, pulmonary lobes, segmentation.

1. INTRODUCTION

The human lung is divided into five functional regions, known as the pulmonary lobes. These compartments are served by separate bronchial and vessel trees, and are largely anatomically independent. Segmenting these lobes from medical imaging data has important applications in treatment planning and regional disease assessment. However, manual segmentation by radiologists is an extremely laborious task, and so there is considerable interest in automated lobar segmentation techniques.

Lobar segmentation in CT scans is commonly achieved through detection of the pulmonary fissures which separate them. This is challenging, since typical intensity values of the fissures are similar to other features in the lung. Parts of the fissures may not be visible due to partial volume effects, and fissures may themselves be incomplete. To overcome these difficulties, *a priori* or anatomical information is generally required to help detect the fissures, which must then be interpolated, extrapolated and combined with the lung boundaries in order to separate the lobes.

Several groups have presented methods for segmentation of all the pulmonary lobes. Van Rikxoort et al. [1] perform an atlas registration, using information derived from the lung borders, airway trees and fissures detected using a supervised filter. Lassen et al. [2] and, independently, Ukil and Reinhardt [3] apply a watershed transform to an image combining CT intensity with a distance transform to the blood vessels. Filter-based fissure detection is incorporated into the watershed transform [2] or as a later refinement step [3]. Some manual correction was required in [3]. Ross et al. [4] use thin plate splines to interpolate a fissure surface from seed points identified by driving a system of particles onto ridge surfaces. Pu et al. [5] use statistical methods to detect fissure points based on the geometric properties of the image, using radial basis functions to generate the final fissure surfaces. Wei et al. [6] search for a planar region of interest free of vessels and airways, and then detect possible fissures using a 2D wavelet transformation. Zhang et al. [7] use an atlas to initialize a ridgeness-based graph searching procedure for the oblique fissures. For both [6] and [7], manually placed markers are required to detect the right transverse fissure.

A number of limitations apply to existing methods. In some cases manual interaction is necessary [3,6,7], which is unsuitable for an automated workflow. Atlas-based approaches [1,7] require training on manually segmented datasets and can be computationally expensive. They may perform poorly on datasets which are not well represented by their training data, such as when the shape and position of the right middle lobe changes in response to disease. Methods which use the vasculature to detect fissure regions [2,3,6] are sensitive to small vessels near the lobar boundaries which could disrupt the segmentations. Those which employ only fissure detection without the use of additional anatomical information may not be robust to incomplete fissures. Finally, lobar segmentation methods can be computationally demanding and authors may resample the images in order to reduce the memory usage and processing time. Resampling can reduce accuracy and introduce imaging artifacts.

The contribution of this paper is to introduce a fully-automated lobar segmentation technique which is computationally efficient, requires no training and is robust both to incomplete fissures and to small vessels crossing the lobar boundaries. Our work extends existing ideas in the field with the following novel aspects: 1) the formulation of a fissureness filter which combines detection of fissure-like structures with suppression of vessel wall structures; 2) the use of a vesselness density filter to create an initial lobar approximation that is robust to small vessels crossing the lobar boundaries; and 3) the use of 3D multilevel B-spline surface-fitting to generate a smooth fissure surface which naturally compensates for incomplete fissures. We present initial results on 10 lung cancer patients.

2. METHODS

In this section we describe our automated method for segmenting the pulmonary lobes. In summary, the method performs the following pipeline: a) Segmentation of the lung parenchyma and identification of the trachea location; b) Segmentation of major airways, centerline finding and determining which lobes they serve; c) Separation of left and right lungs after removing the trachea; d) Identification of blood vessels within the lungs using a vesselness density filter and generation of approximate fissure planes using a watershed transform; e) Calculation of a fissureness measure based on a combination between the eigenvalues of the Hessian matrix and suppression of points close to blood vessels; f) Detection of fissureness maxima in regions of interest near to the approximate fissure planes; and g) Computation of a smooth fissure surface using a multilevel B-spline approximation. This pipeline is illustrated in Fig. 1, and the steps are discussed in detail below.

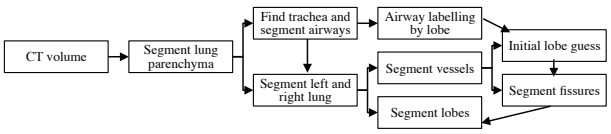


Fig. 1. A simplified illustration of the lobe segmentation pipeline.

2.1. Lung Segmentation and Trachea Location

To extract the lung parenchyma and airways we use a method comprising a noise-reducing 3D Gaussian filter, a thresholding operation (-775 Hounsfield Units) and the automated identification of 3D connected components. To identify the location of the trachea, required as a starting point for airway segmentation, connected components are identified independently in each axial slice of the lung parenchyma segmentation, and components larger than 80mm are removed (the characteristic trachea width being ~40mm). The largest 3D connected component is identified as a section of the trachea and corrected using morphological closing.

2.2. Airway Segmentation and Labeling by Lobe

Starting from the trachea location, we employ a region growing technique with a specifically designed algorithm for explosion control, which corrects for "leakage" across the airway walls at low-intensity voxels. Starting at the top of the trachea, region growing proceeds by evolution of a wavefront, with bifurcations detected by the presence of wavefront splits. Correct evolution of the segmented airway is characterized by wavefront sizes gradually decreasing except for small temporary increases around bifurcation points. If the wavefront size increases above a variable threshold (explosion), it is assumed that it has broken into the lung parenchyma and the current candidate bronchus is discarded. We choose the threshold as five times the minimum wavefront size attained along the airway path from the trachea to the current point.

Once the region growing has been completed and explosions discarded, the airway tree is reduced to a single-voxel centerline using skeletonisation. The branching structure of this tree is analyzed to identify the three right and two left lobar bronchi. This is done by identifying coordinates of subtree centroids, and comparing relative left-to-right and top-to-bottom locations. Subtrees arising from each of the lobar bronchi are assigned to the corresponding lobe.

2.3. Separation of Left and Right Lungs

Left and right lungs are identified as the two connected components remaining after removing the trachea and main left and right bronchi using the segmentation obtained above. If necessary, the two components are separated using a procedure based on morphological erosion. Morphological closing using a spherical structuring element of diameter 8mm is applied to the resulting binary segmentations in order to fill holes and smooth the lung contours.

2.4. Vessel Segmentation and Approximate Fissure Planes using Vesselness Density Watershed

For vessel detection, the Hessian matrix-based vesselness filter introduced in [8] is first calculated, using multiple scales (0.5, 1.0, 1.5, and 2.0mm). A "vesselness density" field is then created by applying a strong (10mm) 3D Gaussian filter to the vesselness filter. A watershed transform is applied to this vesselness density to separate the image into lobe approximations. Each lobar region is seeded using points from the airway tree that have been assigned to that lobe using the airway labeling, excluding the major airway generations. The boundaries between the resulting watershed regions provide our estimation for each fissure.

Our watershed approach differs from existing work [2, 3], where the watershed is applied to a distance transform from the vessels. The distance transform is sensitive to small vessels which can approach or even cross the lobar

boundaries, leading to erroneous segmentations. This is one reason why manual correction is sometimes required [3]. In contrast, the vesselness density is a much smoother function with minima close to the fissure boundaries.

2.5. Fissureness

We have developed a filter analogous to vesselness, which provides a strong response in the vicinity of fissures. We apply a Gaussian filter to the original CT data with a kernel size of 1.5mm, which is an appropriate scale to capture the features of the fissure plane. At each image point the Hessian matrix is constructed. Its eigenvalues λ_1, λ_2, λ_3 are computed and ordered such that $|\lambda_1| \leq |\lambda_2| \leq |\lambda_3|$. At each point we define the fissureness as follows:

$$\mathcal{F} = \Gamma\, \mathcal{F}_{plane}\, \mathcal{F}_{wall}\, \mathcal{F}_{vessels}\,. \tag{1}$$

The first factor suppresses points whose largest eigenvalue λ_3 is positive, since fissures are locally bright:

$$\Gamma = \begin{cases} 1, & \lambda_3 < 0 \\ 0, & \lambda_3 \geq 0 \end{cases}. \tag{2}$$

The second factor detects plane or curve-like structures by searching for locations where the two largest eigenvalues are significantly different:

$$\mathcal{F}_{plane} = \exp\left(-\frac{\mathcal{R}_{plane}{}^2}{2p^2}\right), \quad \mathcal{R}_{plane} = \frac{|\lambda_2|}{|\lambda_3|}, \tag{3}$$

with p (set to 0.5 in our case) acting as a soft threshold on $\mathcal{R}_{plane}$. The third factor suppresses signals from vessel walls, which, in contrast to plane-like fissures, have relatively large second, and possibly also third, eigenvalues. A soft threshold parameter w is used, in this case set to 3:

$$\mathcal{F}_{wall} = \exp\left(-\frac{\mathcal{R}_{wall}{}^2}{2w^2}\right), \quad \mathcal{R}_{wall} = \sqrt{\lambda_1^2 + \lambda_2^2}\,. \tag{4}$$

The final term decreases the fissureness value at points in the vicinity of blood vessels:

$$\mathcal{F}_{vessels} = \exp\left(1 - \frac{DT\{vessels\}^2}{2v^2}\right), \tag{5}$$

Here $DT\{vessels\}$ is the distance transform to segmented blood vessels, found by thresholding the vesselness filter described above. The idea is to suppress points in the vessel walls that are not detected by the wall term because they locally appear plane-like. They are detected because they are close to high-vesselness pixels in the vessel interior. v is a characteristic distance over which fissureness should be suppressed close to vessels. We set v to 5mm. A sample fissureness output is shown in Fig. 2B.

2.6. Fissure surface construction

We represent each fissure as a function $\boldsymbol{f}(\boldsymbol{x}', \boldsymbol{y}')$ where *x'* and *y'* are defined on a fissure estimation plane described below, and $\boldsymbol{f}(\boldsymbol{x}', \boldsymbol{y}')$ is the coordinate $\boldsymbol{z}'$ of the fissure surface on an axis perpendicular to the plane at point $(\boldsymbol{x}', \boldsymbol{y}')$. The function $\boldsymbol{f}(\boldsymbol{x}', \boldsymbol{y}')$ corresponding to the fissure is the one that maximizes the value $\boldsymbol{\mathcal{F}}$ of fissureness over a set of candidate points $\{\boldsymbol{p}\}$ for $\boldsymbol{z}'$ at each value of $(\boldsymbol{x}', \boldsymbol{y}')$:

$$\boldsymbol{f}(\boldsymbol{x}', \boldsymbol{y}') = \underset{\{\boldsymbol{p}\}}{\operatorname{argmin}}\, \boldsymbol{\mathcal{F}}(\boldsymbol{x}', \boldsymbol{y}', \boldsymbol{z}')\,, \tag{6}$$

The candidate points are selected as points within a certain distance (20mm) of the initial lobar boundary approximation generated using the vesselness density watershed method above. The coordinates of each candidate are transformed to the $(\boldsymbol{x}', \boldsymbol{y}')$ basis and grouped into 'bins' corresponding to each value $(\boldsymbol{x}', \boldsymbol{y}')$. Within each bin the candidate voxel with the highest fissureness $\boldsymbol{\mathcal{F}}$ is selected. In this way we keep our image in its original coordinate system, avoiding resampling and interpolation errors.

The estimation plane $(\boldsymbol{x}', \boldsymbol{y}')$ is initially computed as a best fit plane from the watershed fissure estimation, found by applying principal component analysis to the points on the initial approximation surface. Once the maxima $\boldsymbol{f}(\boldsymbol{x}', \boldsymbol{y}')$ have been found, outliers are removed by examining the connectedness of the plane after a morphological dilation using a 3x3x3 voxel cube structural element. Connected components comprising fewer than 200 voxels are removed. The estimation of fissure plane and removal of outliers is carried out in an iterative way. Finally, the resulting surface points are used to compute a smooth fissure surface using a multilevel B-spline method [9] with a thin-plate spline used to extrapolate the values to the lung boundaries.

2.7. Data

CT images were retrospectively obtained for 10 lung cancer patients. Typical tube current-time products were 170mAs. Images were taken after contrast injection on a GE Lightspeed Ultra CT scanner. Images are 512x512 pixels with a pixel resolution of 0.68mmx0.68mm and slice thickness and inter-slice distance of 0.63mm.

2.8. Validation

For each CT dataset, an experienced pulmonary clinician created a gold standard by manually placing fissure markers on every 10th plane. This generated approximately 300 fissure points per dataset. Markers were placed across the whole span of the fissure present in each slice, including points close to the lung boundaries.

3. RESULTS

Table 1 shows validation results for each of the 10 datasets. For comparison with other works, e.g. [1,3,4,7], we quote the mean, maximum and RMS distance in mm of the manually segmented marker points to the nearest point on the automatic fissure segmentation. Fig. 2 illustrates the

output of the fissureness filter and lobe segmentation for Patient 10. Typical execution time for the complete workflow of Fig. 1 is under 10 minutes on a 2.66GHz MacBook Pro running OS 10.7 and Matlab R2011b.

4. DISCUSSION AND CONCLUSION

We have presented a fully-automated, computationally efficient method for segmenting the pulmonary lobes, based on a fissureness filter combining image appearance and anatomical information from the pulmonary vasculature and airways. This anatomical information allows the algorithm to produce a continuous plane even in the absence of clearly defined features in the image. We achieve this using an adaptive minimization plane and a multilevel B-spline fitting. Furthermore, we have found the combination of several information sources adds robustness to the detection, e.g. in the case of small vessels crossing the lobe boundary which are compensated by the presence of other anatomical clues. In general the method does not depend on the quality of the vessel and airway segmentations, since these are only used as an initialization step for the fissure detection. However, as with other published methods [1,2,3,7], our algorithm does require the airway segmentation to correctly find and label the main airway serving each lobe.

The method has been validated quantitatively on a database of lung cancer patients. For oblique fissures, the mean distances are typically <3mm, comparable to other published results [1,3,4,6,7]. We expect higher values for the right transverse fissure, since this fissure is much harder to detect, and some existing methods require manual correction for this fissure [3,6,7]. Our results are broadly within the range of reported inter-observer variability [1,2,4]. However, for some subjects we have found relatively high maximum and RMS values, resulting from inaccurate curve extrapolation near to lung boundaries in regions with poor fissure detection. This is an area we seek to improve. We are currently in the process of increasing the size of the database and including other pathologies.

Fissure	Right oblique			Right transverse			Left oblique		
	Mean	Max	RMS	Mean	Max	RMS	Mean	Max	RMS
Patient 1	3.48	26.2	6.63	1.59	5.47	2.28	2.56	30.3	5.74
Patient 2	2.74	125.	10.4	2.85	9.79	4.35	1.35	14.9	2.86
Patient 3	2.35	17.6	3.82	7.52	16.1	9.06	2.12	26.6	4.22
Patient 4	1.62	16.2	2.96	3.78	15.9	6.02	1.22	8.97	2.16
Patient 5	2.56	31.0	4.62	3.60	12.6	5.00	1.97	12.1	2.99
Patient 6	2.73	14.1	3.81	3.63	11.9	5.01	2.81	19.0	4.41
Patient 7	3.59	16.9	5.05	3.30	12.9	4.80	2.67	14.4	3.62
Patient 8	1.16	10.4	1.95	3.60	9.40	4.75	1.44	16.4	2.81
Patient 9	2.99	21.4	4.42	4.45	17.9	6.45	1.79	15.4	3.09
Patient 10	2.70	20.8	4.81	4.47	15.4	6.71	3.16	28.6	6.12

Table 1. Validation results for fissure detection, grouped by fissure. We show mean, max and root mean square of the distance in mm from a set of manually segmented fissure points to the nearest point on the automatically segmented fissure curve.

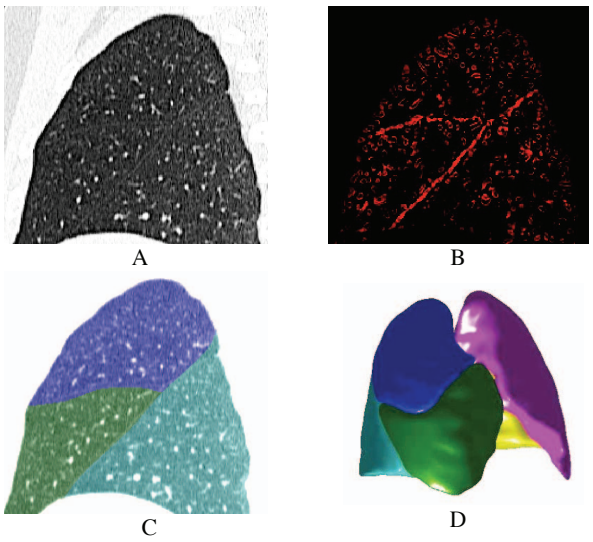


Fig. 2. Results for patient 10. A) Sample slice from the original CT density image. B) Output of the fissureness filter for this slice. C) Slice overlaid by the automatic lobar segmentation. D) 3D surface rendering of the resulting lobar segmentation.

5. REFERENCES

[1] E. M. van Rikxoort et al., "Automatic Segmentation of Pulmonary Lobes Robust Against Incomplete Fissures," IEEE Trans. Med. Imag., vol. 29, no. 6, pp. 1286-1296, 2010.

[2] B. Lassen et al., "Automatic Segmentation of Lung Lobes in CT Images Based on Fissures, Vessels, and Bronchi," IEEE International Symposium on Biomedical Imaging: From Nano to Macro, pp. 560-563, 2010.

[3] S. Ukil, J. M. Reinhardt, "Anatomy-Guided Lung Lobe Segmentation in X-Ray CT Images," IEEE Trans. Med. Imag., vol. 28, no. 2, pp. 202-214, 2009.

[4] J. C. Ross et al, "Automatic Lung Lobe Segmentation Using Particles, Thin Plate Splines, and Maximum a Posteriori Estimation," MICCAI 2010, vol. 6363, pp. 163-171, 2010.

[5] J. Pu, et al., "Pulmonary Lobe Segmentation in CT Examinations Using Implicit Surface Fitting," IEEE Trans. Med. Imag., vol 28, no. 12, pp. 1986-1996, 2009.

[6] Q. Wei et al., "Segmentation of Lung Lobes in High-Resolution Isotropic CT Images," IEEE Trans. Biomed. Eng., vol. 56, no. 5, pp. 1383-1393, 2009.

[7] L. Zhang et al., "Atlas-Driven Lung Lobe Segmentation in Volumetric X-Ray CT Images," IEE Trans. Med. Imag., vol. 25, no. 1, pp. 1-16, 2006.

[8] A. F. Frangi et al., "Multiscale Vessel Enhancement Filtering," MICCAI 1998, vol. 1496., pp. 130-137, 1998.

[9] S. Lee et al., "Scattered Data Interpolation with Multilevel B-Splines," IEEE Trans. Vis. Comput. Graph., vol. 3, no. 3, pp. 228-244, 1997.